Available online at www.sciencedirect.com
SCIENCE DIRECT®
Thermochimica Acta 403 (2003) 275–285
thermochimica acta
www.elsevier.com/locate/tca

Thermodynamic modelling of the O–Sn system

S. Cahen, N. David, J.M. Fiorani, A. Maître, M. Vilasi*

Thermodynamique et Corrosion Group, Laboratoire de Chimie du Solide Minéral, UMR CNRS 7555-BP 239, Université Henri Poincaré-Nancy 1, Vandoeuvre-les-Nancy Cedex F-54506, France

Received 28 October 2002; received in revised form 10 January 2003; accepted 17 January 2003

Abstract

Thermodynamic and phase diagram data relative to the O–Sn system have been assessed. The existence, the type and the temperature of invariant equilibria $Melt1_{(l)} \rightleftharpoons Melt2_{(l)} + SnO_{2(s)}$ and $Sn_3O_{4(s)} \rightleftharpoons 2SnO_{(s)} + SnO_{2(s)}$ have been the subject of DSC and XRD experiments. The adjustable parameters of the modelling are obtained by the CALculation of PHAse Diagram (CALPHAD) method fitted thanks to diagram and thermodynamic data through Thermo-Calc^{TM} software. In particular, the liquid phase is described by the way of the Hillert's partially ionic liquid model. The final result is in good agreement with all of the experimental data available. Activities of tin and oxygen versus composition at different high temperatures can be calculated.

Keywords: Thermodynamic modelling; O–Sn system; DSC and XRD experiments; Ionic liquid model

1. Introduction

In the course for the development of new fully densified ceramic materials for industrial applications, we have focused our attention on ZrO_2–SnO_2-based ceramics. These materials are already used for specific applications such as heating electrodes or oven bricks. However, it appeared that ceramics commercially available present a low corrosion resistance versus molten silicate slag, as they contain glass-bonds. Moreover, the decomposition of SnO_2 [1,2] at temperature higher than 1573 K according to Eq. (1) must be taken into account:

$$SnO_{2(s)} \rightarrow SnO_{(g)} + \tfrac{1}{2}O_{2(g)} \quad (1)$$

Furthermore, SnO_2 has an oxidising capability that could generate its reduction into liquid metallic tin in presence of metals or metallic compounds. So, the knowledge of the tin activity versus temperature and composition seemed to be the mean for evaluating oxidising capability of the new SnO_2-based materials. Moreover, it appeared necessary to optimise the chemical composition of these ceramic materials, especially for avoiding or at least for limiting their volatilisation. Therefore, the experimental phase diagram O–Sn–Zr has been studied between 1503 and 2023 K [3]. Unfortunately, the results obtained are complete because of experimental difficulties met at the higher temperatures (>2023 K). In order to overcome those difficulties, a thermodynamic modelling of the O–Sn–Zr system could be performed through the CALculation of PHAse Diagram (CALPHAD) method [4]. A bibliographic review showed that O–Zr [5–7] and Sn–Zr [8] systems had been already modelled, unlike O–Sn which is also necessary for the thermodynamic evaluation of the O–Sn–Zr system.

* Corresponding author. Fax: +33-383-368-4611.
E-mail address: michel.vilasi@lcsm.uhp-nancy.fr (M. Vilasi).

0040-6031/03/$ – see front matter © 2003 Elsevier B.V. All rights reserved.
doi:10.1016/S0040-6031(03)00059-5

Thus, the aim of the present work is to provide a thermodynamic modelling of the O–Sn system. This task has needed to consider the whole diagram and thermodynamic data, which revealed a lack of data for certain composition range.

2. Background

Stannic oxide appearing on this diagram is widely used for technological applications. It is n-type semiconductor presenting a large gap and is generally used as specific oxygen gas sensor or photo-detector. The corresponding O–Sn phase diagram has been the subject of contradictory studies [9–48]. Table 1 presents the whole crystallographic data of solid phases in the O–Sn system. Oxides in this table are presented as stoichiometric.

Nevertheless, their results allow describing roughly this system in two parts related to the temperature range. Between 298 and 1273 K, the system is characterised by the experimental phase diagram established by Moh [9] which is presented in Fig. 1. Moh [9] indicates that SnO exists in its stable state from 298 up to about 543 K. This latter compound crystallises in the tetragonal symmetry confirmed elsewhere by many authors [10–13]. Nevertheless, we can note that an other orthorhombic variety had been suggested by Donaldson et al. [14,15]. According to this diagram, we can also notice that Sn_3O_4 is a stable compound between 723 K and a lower temperature which will be determined in this work. This

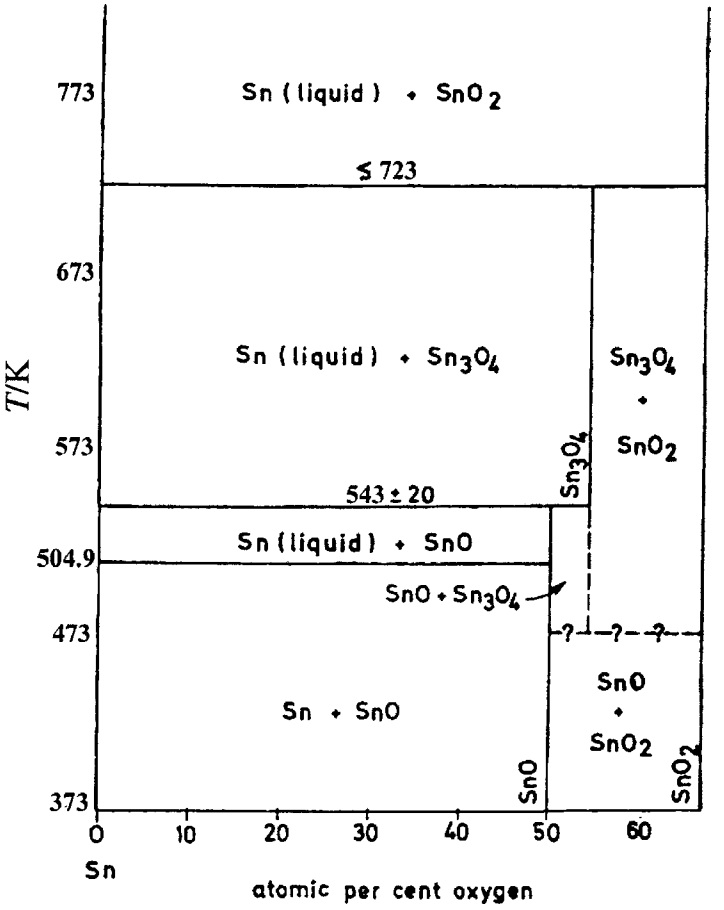

Fig. 1. O–Sn phase diagram established by Moh [9].

Table 1
Crystallographic data of the O–Sn system

Phase	Composition (O at.%)	Space group	Pearson symbol	Prototype	Reference
α-Sn	0	$Fd\bar{3}m$	cF8	C (diamond)	[18]
β-Sn	<0.01	$I4_1/amd$	tI4	β-Sn	[18]
SnO	50	$P4/nmm$	tP4	PbO	[18]
Sn_3O_4	57.1	P (not assigned)	a (not assigned)	Sn_3O_4	[16]
SnO_2	66.7	$P4_2/mnm$	tP6	TiO_2	[18]

compound is considered to be of triclinic symmetry [16]. Finally, SnO_2 which is confirmed by Baur and Kahn [17] to adopt a tetragonal symmetry, is stable from room temperature to the higher temperatures.

Between 1273 and 3500 K, the binary phase diagram describing the O–Sn system is the hypothetical one proposed by McPherson and Hanson [18] and still presented by Massalski [19] (see Fig. 2). On this diagram, we can note that SnO_2 melts congruently at about 2273 K. The liquid phase exhibits a large miscibility gap over a temperature measured at 1313 K by McPherson and Hanson [18] and at 1353 K by Kuxmann and Dobner [20]. This temperature will be precised through DSC measurements in this work.The gas phase presented by McPherson and Hanson [18] contains many species identified by different authors [22–24].

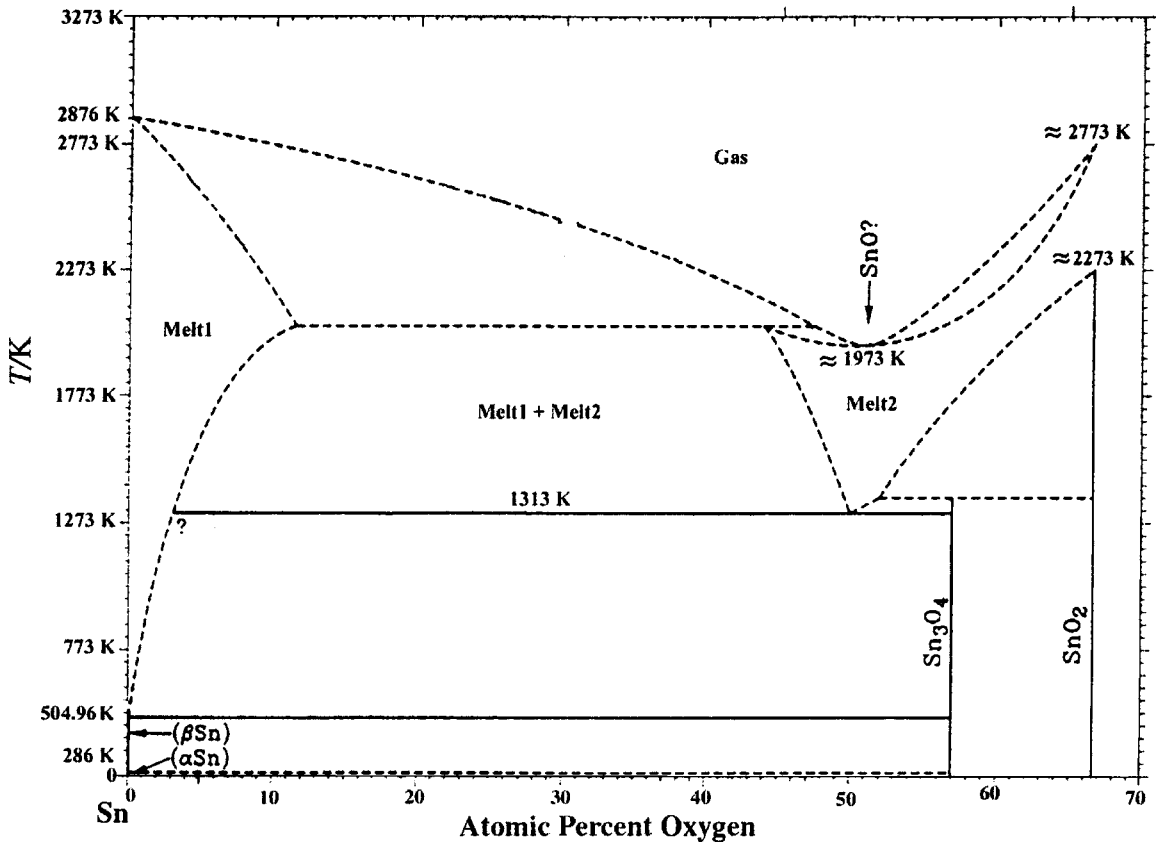

Fig. 2. O–Sn phase diagram proposed by McPherson and Hanson [18].

3. Experimental

3.1. Experimental data from literature

3.1.1. Tin oxides

Through electrochemical measurements carried out between room temperature and 1823 K, Schaefer [25] and Bannister [26] have determined Gibbs energy values relative to the SnO_2 formation. We can note that all equations determined by these authors are equivalent.

Li-Zi et al. [27], using emf measurements, have evaluated Gibbs energy values relative to Sn_3O_4 between 696 and 731 K. The temperature of Sn_3O_4 decomposition at low temperature is yet unknown and will be determined in this work.

Entropy and enthalpy values of SnO formation between room temperature and 1773 K are given in Barin tables [28].

3.1.2. Liquid phase

All of the O–Sn phase diagrams taken from literature show a large miscibility gap in the liquid phase. Two different liquids can be identified: the first one is a tin-rich liquid called "Melt1" whereas the second one seems to present a composition close to the one of SnO and that will be denoted "Melt2".

Some electrochemical measurements [29–33,39–44] allowed the determination of the activity of oxygen in liquid tin between 773 and 1373 K.

3.1.3. Gas phase

The gas phase described in this work will be considered as constituted of the different species Sn, Sn_2, O, O_2, O_3, SnO, SnO_2, Sn_2O_2, Sn_4O_4 and Sn_6O_6. The database used by Thermo-Calc^{TM} in order to describe the gas phase was optimised with polycondensed species. These latter were found in a high temperature study by Zimmerman et al. [22,23] using mass spectroscopy and Knudsen effusion cell.

3.2. Experimental data from this work

In order to perform the experimental study of the O–Sn phase diagram, we used different powders of:

- Sn provided by Descharmes & C^{ie} with a purity of about 99.99%;
- SnO_2, provided by Chempur^{TM} with a purity of about 99%;
- SnO, furnished by Aldrich with a purity of about 99%.

After mixing and thermal treatments, samples were characterised by several techniques:

- Some XRD measurements were performed by means of two different diffractometers. The first one is a PHILIPS X'Pert Pro with a Cu Kα1 source ($\lambda = 1.54056$ Å) in the Bragg–Brentano θ–2θ geometry. It was used in order to get X-ray patterns in a high temperature range. The second one is a CGRθ60 diffractometer also equipped with a Cu anti-cathode. It was used to perform XRD characterisations at room temperature. Diffractograms were then studied by the way of the Diffract-AT software [34].
- Calorimetric experiments were done using two calorimeters: a microcalorimeter (Sceres-type) for the low temperature range, and a second one developped in the laboratory [35] and particularly adapted for high temperature measurements (>1273 K).

3.2.1. Invariant equilibrium $Sn_3O_{4(s)} \rightleftharpoons SnO_{2(s)} + 2SnO_{(s)}$

Some experiments were undertaken in the lower temperature part of the phase diagram in order to determine the existence, the type and the temperature of the invariant equilibrium suggested by Moh [9] according to Eq. (2):

$$Sn_3O_{4(s)} \rightleftharpoons 2SnO_{(s)} + SnO_{2(s)} \quad (2)$$

Towards characterising this reaction, a sample of molar composition $x(O) = 0.6$ is prepared from a mixture of SnO and SnO_2 oxides ground in an agate mortar. X-ray experiments are performed by steps of 50 K, from 673 to 373 K. The experiment was carried out with a 0.02° Bragg's angle step, angle maintained constant during 16 s. Diffractograms so obtained are presented in Fig. 3. They indicate that, between 673 and 423 K, phases in equilibrium are ever Sn_3O_4 and SnO_2, identified with the aid of the JCPDS file [34]. The results of DSC measurements (performed with the Sceres-type calorimeter) are presented in Fig. 4. They reveal the existence of two exothermic reactions at 410 and 386 K. On one hand, the temperature of 410 K can be associated with the monotectic reac-

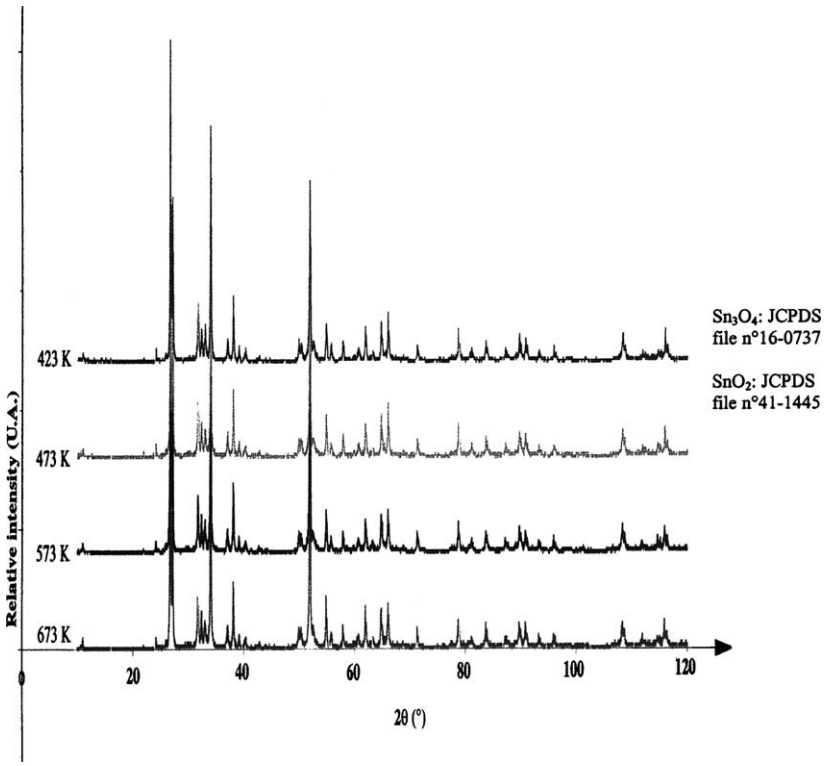

Fig. 3. X-ray patterns of a Sn_3O_4–SnO_2 mixture obtained at different temperatures. Each peak can be indexed thanks to JCPDS files corresponding to Sn_3O_4 or SnO_2.

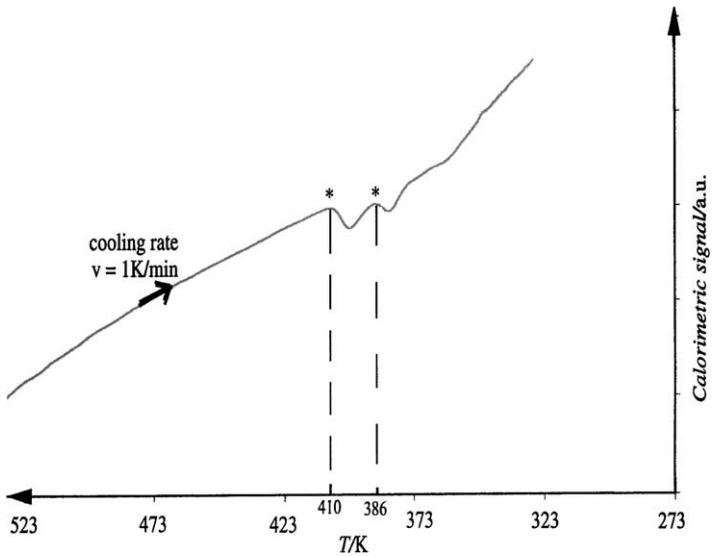

Fig. 4. DSC experiments performed for a sample $x(O) = 0.6$ with a cooling rate of 1 K/min. Dash lines show the beginning of reactions.

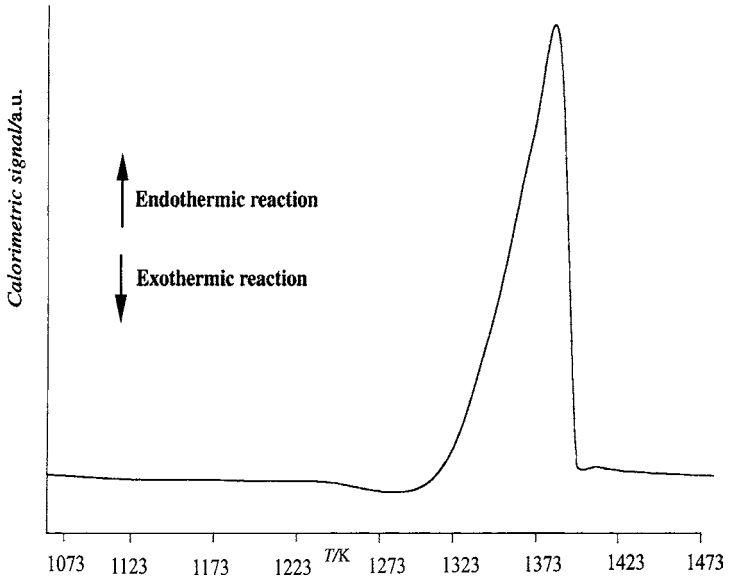

Fig. 5. DSC experiment performed at high temperatures.

tion of Eq. (2). On another hand, the reaction occurring at 386 K had not been identified yet. It generates two different phases in equilibrium. The first one could be identified as SnO_2 by the JCPDS file [34], but the other one remains undetermined. Afterwards, a thermal treatment of 60 h at 373 K was performed in order to complete the transformation of Sn_3O_4. The annealed sample was quenched in water and then analysed by XRD techniques at room temperature. The results showed the presence of two oxides: SnO_2 previously observed, and an other phase that was not identified yet. This latter could be assimilated with a new allotropic variety of SnO. This phase is a new one which can not be indexed by means of JCPDS data file.

3.2.2. Invariant equilibrium $Melt2_{(l)} \rightleftharpoons Melt1_{(l)} + SnO_{2(s)}$ at high temperature

As mentioned before, the temperature of the monotectic reaction of Eq. (3) is not exactly known. Moreover, according to the results obtained by Moh [9], the invariant equilibrium leads to the formation of SnO_2 and not of Sn_3O_4 as indicated by McPherson and Hanson [18] (Fig. 2).

$$Melt2_{(1)} \rightleftharpoons Melt1_{(1)} + SnO_{2(s)} \quad (3)$$

Therefore, some complementary experiments have been performed during this work. A sample of molar composition $x(O) = 0.2$ was prepared from Sn and SnO_2 powders ground in an agate mortar. In order to determine the reaction temperature, a DSC experiment was done by means of the high temperature calorimeter and the corresponding result is reported in Fig. 5. Thus, the temperature of the monotectic reaction (3) occurs at 1313 ± 2 K.

4. Thermodynamic models

4.1. Pure elements

The Gibbs energy of a pure element i, ${}^0G_i(T)$, referred to the enthalpy of formation in its stable state (SER) at 298.15 K and 1 bar, H_i^{SER} (298.15 K), is described as a function of the temperature by the following equation:

$$\begin{aligned} {}^0G_i(T) - H_i^{SER}(298.15\,K) &= a + bT + cT\ln T + dT^2 + eT^{-1} + fT^3 \\ &\quad + iT^7 + jT^{-9} \end{aligned} \quad (4)$$

The values of the used parameters a to j are those published by Dinsdale [36].

4.2. Intermediate compounds: SnO, Sn_3O_4 and SnO_2

These oxides are described by the sublattice model [4,49]. In the O–Sn system, all oxides studied are considered as stoichiometric compounds as suggested by the literature [9,18]. The molar Gibbs energy of phases, denoted by the subscript ϕ, is expressed as follows:

$$G^{\phi} - H^{\mathrm{SER}} = a + bT \tag{5}$$

where H^{SER} is an abbreviation for $\sum_i x_i H_i^{\mathrm{SER}}$ (298.15 K), and a and b are adjustable coefficients.

4.3. Liquid phase

The liquid phase was modelled with Hillert's partially ionic liquid model [4,37], assuming tetravalent tin ions on the cation "sublattice" and divalent oxygen ions, vacancies (having charge −4 in this system) and neutral oxygen atoms on the anion "sublattice".

The general occupancy of the two "sublattices" can be written as $(Sn^{4+})_P(V^{4-}, O^{2-}, O)_Q$ where P and Q are the site numbers of each sublattice in the ionic liquid model. In the case of the O–Sn system, $Q = 4$ and $P = 4y_{V^{4-}} + 2y_{O^{2-}}$. The Gibbs energy for 1 mol of formula units is given following Eq. (6) as:

$$\begin{aligned} G^{\mathrm{liq}} - H^{\mathrm{SER}} &= y_{V^{4-}} Q(G^{\mathrm{liq}}_{\mathrm{Sn}} - H^{\mathrm{SER}}_{\mathrm{Sn}}) + y_{O^{2-}}({}^0G^{\mathrm{liq}}_{Sn^{4+}:O^{2-}} \\ &\quad -2H^{\mathrm{SER}}_{\mathrm{Sn}} - 4H^{\mathrm{SER}}_{\mathrm{O}}) + y_{\mathrm{O}} Q({}^0G^{\mathrm{liq}}_{\mathrm{O}} - H^{\mathrm{SER}}_{\mathrm{O}}) \\ &\quad + RTQ(y_{V^{4-}} \ln y_{V^{4-}} + y_{O^{2-}} \ln y_{O^{2-}} + y_{\mathrm{O}} \ln y_{\mathrm{O}}) \\ &\quad + y_{V^{4-}} y_{O^{2-}} \{{}^0L^{\mathrm{liq}}_{Sn^{4+}:V^{4-},O^{2-}} \\ &\quad + {}^1L^{\mathrm{liq}}_{Sn^{4+}:V^{4-},O^{2-}}(y_{V^{4-}} - y_{O^{2-}})\} \\ &\quad + y_{V^{4-}} y_{\mathrm{O}} {}^0L^{\mathrm{liq}}_{Sn^{4+}:V^{4-},O} + y_{O^{2-}} y_{\mathrm{O}} {}^0L^{\mathrm{liq}}_{Sn^{4+}:O^{2-},O} \end{aligned} \tag{6}$$

where $y_{V^{4-}}$, $y_{O^{2-}}$ and y_{O} denote the site fractions of vacancies, divalent oxygen ions and neutral oxygen, respectively, on the anion sublattice. If only neutral oxygen atoms "O" exist on the anion sublattice, $P = 0$. Therefore, the symbol ${}^0G^{\mathrm{liq}}_{\mathrm{O}}$ does not contain "Sn^{4+}:" in the subscript.

$(G^{\mathrm{liq}}_{\mathrm{Sn}} - H^{\mathrm{SER}}_{\mathrm{Sn}})$ and $({}^0G^{\mathrm{liq}}_{\mathrm{O}} - H^{\mathrm{SER}}_{\mathrm{O}})$ represent the Gibbs energies of 1 mol of liquid Sn atoms and fictitious pure liquid oxygen atoms, respectively. $({}^0G_{Sn^{4+}:O^{2-}} - 2H^{\mathrm{SER}}_{\mathrm{Sn}} - 4H^{\mathrm{SER}}_{\mathrm{O}})$ represents the molar Gibbs energy of the ideal hypothetical liquid Sn_2O_4. ${}^vL$ are interaction parameters of v order, between Sn^{4+} and i and j species.

4.4. Gas phase

The gas phase is treated in this study as an ideal mixture [4] containing the following species: Sn, Sn_2,

Table 2
Thermodynamic data used for modelling the O–Sn system

Data type	Reference	Experimental technique
Temperature of the reaction: $Sn_3O_4 \rightleftharpoons 2SnO + SnO_2$	This work	DSC + XRD
Temperature of the reaction: Melt1 + $SnO_2 \rightleftharpoons$ Melt2	This work	DSC + XRD
Oxygen solubility	[31]	Emf measurements
Oxygen solubility	[20]	Emf measurements
Oxygen solubility	[27]	Emf measurements
Gibbs energy of formation of SnO_2	[25,26]	Emf measurements
Gibbs energy of formation of Sn_3O_4	[27]	Emf measurements
Gibbs energy of formation of SnO	[28]	Calorimetric measurements
Composition of the gas phase	[22,23]	Mass spectrometry

O, O_2, O_3, SnO, SnO_2, Sn_2O_2, Sn_4O_4 and Sn_6O_6. The Gibbs energy for 1 mol of formula unit is given as (see Eq. (7)):

$$G^{\text{gas}}(T, P) = \sum_i y_i \{{}^0G_i^{\text{gas}} + RT\ln(y_i)\} + RT\ln P \quad (7)$$

where y_i is the mole fraction of species i in the gas phase, and ${}^0G_i^{\text{gas}}$ its molar Gibbs energy. P gives the total pressure and R is the gas constant.

A thermodynamic description of the O–Sn gas phase has recently been given by Zimmerman et al. [22,23]. In this work, the type of polynoms used to represent the Gibbs energy are those given in the SGTE substance database [24] for the species Sn, Sn_2, SnO, SnO_2, O, O_2, O_3. The functions for SnO, SnO_2, Sn_2O_2, S_4O_4 and Sn_6O_6 were then readjusted to be consistent with the whole diagram and thermodynamic data available concerning the gas phase of the O–Sn system.

4.5. Primary solid solutions α-Sn (C (diamond)) and β-Sn (bct)

α-Sn and β-Sn are described following the sublattice model. Regarding to the lack of information relative to the oxygen solubility in tin, this will be considered as equal to zero, therefore no adjustable parameters were calculated during the modelling of these phases.

5. Modelling of the O–Sn system

The whole thermodynamic data relative to the O–Sn system and used for the modelling are presented in Table 2. After fitting of the adjustable parameters, the phase diagram finally obtained is presented in Fig. 6. The corresponding calculated adjustable parameters are reported in Table 3. In order to validate the present modelling, known phase diagram and thermodynamic data can be used.

First, we can compare the calculated phase diagram with the one proposed by McPherson and Hanson [18] in the temperature range 1273–3500 K. These phase diagrams seem to be similar. If we compare the calculated phase diagram with the one determined by Moh [9] in the low temperature range (298–1273 K), both are equivalent. Moreover, the present modelling takes into account the invariant reaction (2) characterised in this work.

Table 3
Optimised parameters of the O–Sn system

Adjustable parameter	$a_{i,j}^{v,\varphi}$	$b_{i,j}^{v,\varphi}$
Liquid, partially ionic liquid $(Sn^{4+})_P(O^{2-}, V^{4-}, O^0)_Q$		
${}^0G_{\text{O}}^{\text{liq}}$	−267770	117.591
${}^0G_{\text{Sn}^{4+}:\text{O}^{2-}}^{\text{liq}}$	−1146086	390.289
${}^0L_{\text{Sn}^{4+}:\text{V}^{4-},\text{O}^{2-}}^{\text{liq}}$	11435	49.612
${}^1L_{\text{Sn}^{4+}:\text{V}^{4-},\text{O}^{2-}}^{\text{liq}}$	−62968	−190.36
${}^0L_{\text{Sn}^{4+}:\text{O}^{2-},\text{O}}^{\text{liq}}$	287667	−167.380
Gas, ideal mixture		
${}^0G_{\text{SnO}}^{\text{gas}}$	−222136	117.626
${}^0G_{\text{SnO}_2}^{\text{gas}}$	117.889	500.036
${}^0G_{\text{Sn}_2\text{O}_2}^{\text{gas}}$	1669493	−109.724
${}^0G_{\text{Sn}_4\text{O}_4}^{\text{gas}}$	877437	6.346
${}^0G_{\text{Sn}_6\text{O}_6}^{\text{gas}}$	−1713003	834.537
Stoichiometric compound (SnO_2)		
${}^0G_{\text{SnO}_2}^{\text{solid}}$	−581195	183.114
Stoichiometric compound (Sn_3O_4)		
${}^0G_{\text{Sn}_3\text{O}_4}^{\text{solid}}$	−1165456	366.142
Stoichiometric compound (Sn_3O_4)		
${}^0G_{\text{SnO}}^{\text{solid}}$	−294112	96.347

Table 4 reviews all the different invariant equilibria, which are well restored by the present modelling.

Table 5 presents enthalpy ($\Delta H_{\text{formaton}}^{\text{Sn}_x\text{O}_y}$) and entropy ($\Delta S_{\text{formaton}}^{\text{Sn}_x\text{O}_y}$) values of formation for the different oxides. From this table, it appears that the results got for SnO are in good agreement with those taken from the literature. For SnO_2 and Sn_3O_4 oxides, thermodynamic values calculated are satisfactory in comparison with the data furnished in the literature. About Sn_3O_4, we can note that the enthalpic and entropic parts are obtained by Li-Zi et al. [27] on a narrow temperature range (35 K) and consequently must be considered carefully.

Values of oxygen activity in liquid tin by Chou et al. [31] are compared with those obtained by the modelling of the O–Sn system (Table 6). The differences between calculated and measured values never exceed

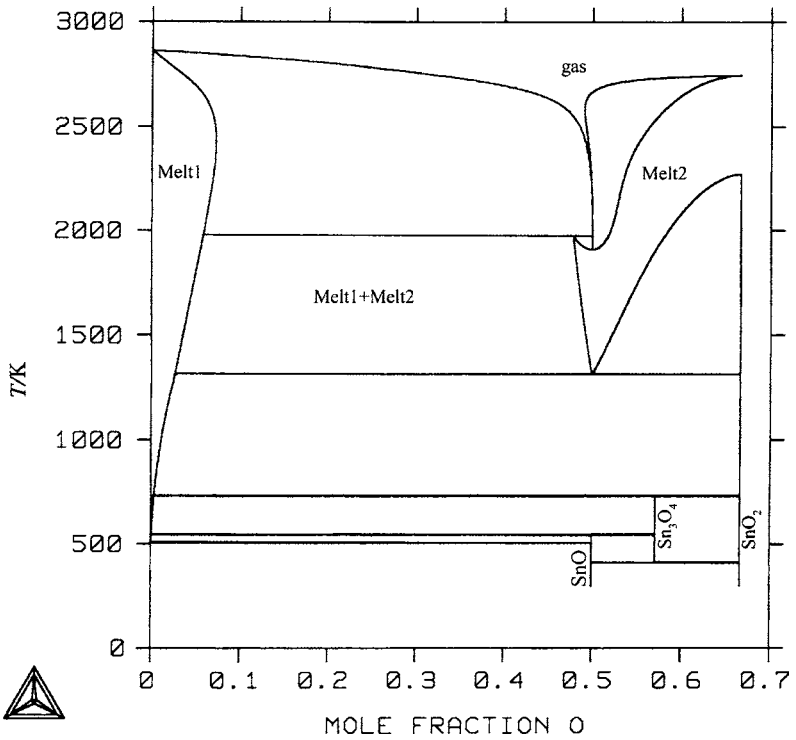

Fig. 6. Final O–Sn phase diagram, calculated at 1 bar.

Table 4
Characteristics of invariant equilibria (composition, temperature) compared with data from literature

Invariant	Composition of phases (O at.%)						T (K)		Reference
	Calculated			From literature			Calculated	From literature	
liq2⇌gas	66.60	?		66.67	?		2746	2800	[18,19]
1iq2⇌gas	49.99	?		50	?		1908	1910	[18,19]
SnO_2⇌liq2	66.67	66.67		66.67	66.67		2272	2273	[18,19]
liq2⇌liq1 + gas	47.85	5.80	?	45.00	10	?	1973	1973	[18,19]
liq1⇌liq2 + SnO_2	2.67	50.01	66.7	3.3	50.30	66.7	1309	1313	[18,19], this work
β − Sn⇌liq1 + SnO	0	4×10^{-4}	50	0	0	50	505.08	504.96	[18,19]
Sn_3O_4⇌liq1 + SnO	57.14	6×10^{-4}	50	57.14	0	50	543.4	543	[9]
SnO_2⇌liq1 + Sn_3O_4	66.67	0.33	57.14	66.67	0.1	57.14	729.8	723	[9]
Sn_3O_4⇌SnO_2 + SnO	57.14	66.67	50	57.14	66.67	50	410	410	[9], this work

Table 5
Values of enthalpy and entropy from the present modelling compared with the literature

Phase	ΔH (J mol^{-1})		Deviation (%)	ΔS (J K^{-1} mol^{-1})		Deviation (%)	Reference
	Calculated	Measured		Calculated	Measured		
SnO_2	−581195	−576077[a]	0.9	183.114	205.245[a]	10.9	[25–27,29,38–48]
Sn_3O_4	−1165456	−1163900	0.2	366.142	417.36	14.0	[26]
SnO	−294112	−285920	2.8	96.347	100.26	4.1	[27]

[a] Average calculated from [25–27,29,38–48].

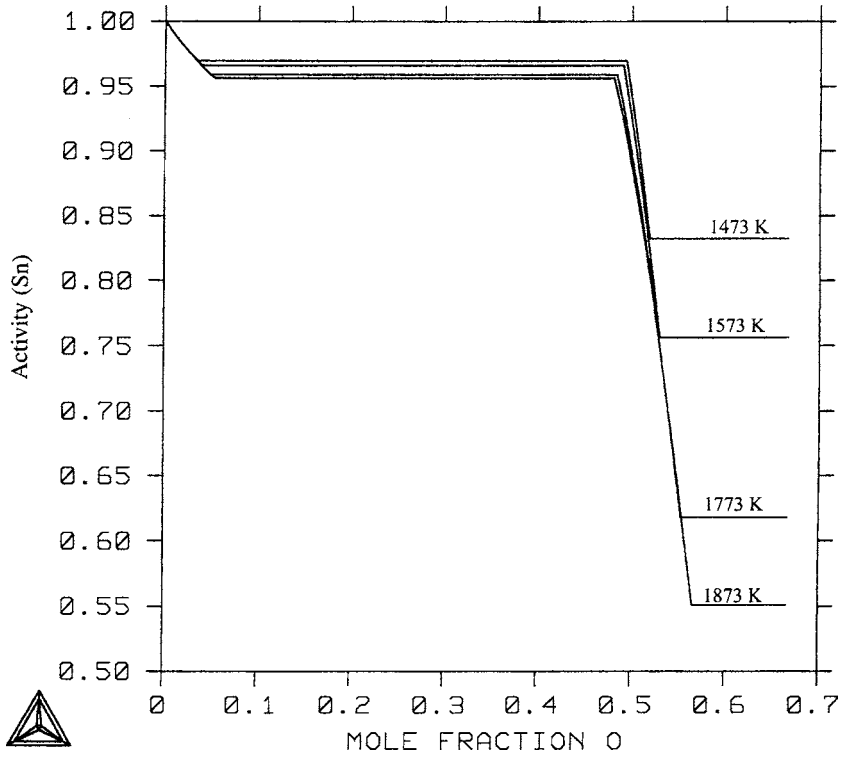

Fig. 7. Tin activity vs. composition for different high temperatures.

3%. The different thermodynamic values (entropies, enthalpies, activities) obtained by the modelling are in good agreement with data taken from the literature and data measured in the present study. This modelling allows an access to information hardly available by experiments. For example, the present modelling can be used in order to predict the activity of tin (Fig. 7) at different temperatures and compositions.

Table 6
Comparison between values of oxygen activity from the present modelling with those determined by Chou et al. [31]

Temperature (K)	Composition (O at.%)	Emf (V)		
		Calculated	From [31]	Deviation (%)
1073	1.77	0.969	0.950	2.0
	1.15	0.986	0.970	1.6
	0.61	1.014	1.000	1.4
1123	4.18	0.918	0.910	0.9
	2.23	0.940	0.940	0.0
	1.21	0.966	0.970	0.4
	0.65	0.993	1.000	0.7
1173	2.05	0.923	0.945	2.4
	1.28	0.944	0.970	2.8
	0.71	0.972	1.000	2.9
	0.26	1.020	1.050	2.9

6. Conclusion

We can conclude that the modelling of the O–Sn system is satisfying because of the good agreement between experimental and calculated thermodynamical values. Nevertheless, it appears necessary to obtain a few complementary experimental information. Especially, we will give a particular attention to the allotropic transformation of SnO at about 386 K. Some further characterisations by SEM and XRD techniques appear necessary to precise the type and the temperature of this invariant reaction.

As the three binary systems are now modelled, it will be possible to perform the modelling of the O–Sn–Zr system. This will then allow the optimisation

of the chemical composition of SnO_2–ZrO_2-based materials in order to obtain a better coherence and consequently resistance of these materials against particular aggressive environments at high temperatures.

References

[1] C.L. Hoenig, A.W. Searcy, J. Am. Ceram. Soc. 49 (1966) 128–134.
[2] E.R. Leite, J.A. Cerri, E. Longo, J.A. Varela, C.A. Paskocima, J. Eur. Ceram. Soc. 21 (2001) 669–675.
[3] B. Gaillard-Allemand, R. Podor, M. Vilasi, C. Rapin, A. Maître, P. Steinmetz, J. Eur. Ceram. Soc. 22 (2002) 2297–2303.
[4] N. Saunders, A.P. Miodownik, Calphad: calculation of phase diagrams, a comprehensive guide, in: R.W. Cahn (Ed.), Pergamon Materials Series, Pergamon Press, Oxford, 1998.
[5] P.Y. Chevalier, E. Fischer, J. Nuc. Mater. 257 (1998) 213–255.
[6] C. Gueneau, V. Dauvois, P. Perodeaud, C. Gonella, O. Dugne, J. Nuc. Mater. 254 (1998) 158.
[7] P. Liang, N. Dupin, S.G. Fries, H.J. Seifert, I. Ansara, H.L. Lukas, F. Aldinger, Z. Metallkd. 92 (2001) 747–756.
[8] N. Subasic, Calphad 22 (1998) 157–165.
[9] G.H. Moh, Chem. Erde 33 (1974) 243–275.
[10] W.J. Moore, L. Pauling, J. Am. Chem. Soc. 63 (1941) 1392.
[11] H.E. Swanson, Can. Mineral. 10 (1971) 916.
[12] J. Pannetier, G. Denes, Acta Crystallogr. B 36 (1980) 2763.
[13] F. Izumi, J. Solid State Chem. 38 (1981) 381.
[14] J.D. Donaldson, W. Moser, W.B. Simpson, J. Chem. Soc. (1961) 830.
[15] J.D. Donaldson, W. Moser, W.B. Simpson, Acta Crystallogr. A 16 (1961) 22.
[16] F. Lawson, Nature 215 (1967) 955.
[17] W.H. Baur, A.A. Kahn, Acta Crystallogr. B 27 (1971) 2133.
[18] D.J. McPherson, M. Hanson, Trans. ASM 45 (1953) 915.
[19] T.B. Massalski (Ed.), in: Binary Alloy Phase Diagram, second ed., vol. 3, American Society for Metals, Ohio, 1990, p. 2920.
[20] U. Kuxmann, R. Dobner, Metallurgy (Berlin) 34 (1980) 821–827.
[21] M. Drabek, M. Stemprok, N. Jb. Miner. Abh. 122 (1973) 90–118.
[22] E. Zimmermann, S. Königs, D. Neuschütz, Z. Phys. Chem. 193 (1996) 195–206.
[23] E. Zimmermann, S. Königs, D. Neuschütz, Z. Phys. Chem. 209 (1999) 271–280.
[24] The SGTE Substance Database, Version 1997, Scientific Group Thermodata Europe (SGTE), Grenoble, France, 1997.
[25] S.C. Schaefer, Invest. US Bur. Mines 8906 (1984) 10.
[26] M.J. Bannister, J. Chem. Thermodyn. 18 (1986) 455–463.
[27] Y. Li-Zi, S. Zhi-Thong, W. Chan-Zheng, J. Solid State Chem. 113 (1994) 221–224.
[28] I. Barin (Ed.), Thermodynarnical Data of Pure Substances, third ed., VCH, Weinheim, 1995, pp. 1549–1550.
[29] T.N. Belford, C.B. Alcock, Trans. Faraday Soc. 61 (1965) 443–453.
[30] J. Carbo Nover, F.D. Richardson, Inst. Mining Met. Trans. 81 (1972) 63–68.
[31] H. Chou, H.S. Chen, W.C. Fang, P.L. Trevor, J. Electrochem. Soc. 139 (1992) 3545–3549.
[32] M.C. Heuzey, A.D. Pelton, Metall. Mater. Trans. B 27 (1996) 810–828.
[33] R. Kurchania, G.M. Kale, J. Mater. Res. 15 (2000) 1576–1582.
[34] P. Caussin, J. Nusinovici, D.W. Beard, Adv. X-Rays Anal. 31 (1988) 423.
[35] J.C. Gachon, Thesis, University of Nancy, France, 1986.
[36] A.T. Dinsdale, Calphad 15 (1991) 317–425.
[37] M. Hillert, B. Jansson, B. Sundman, J. Ågren, Met. Trans. A 16 (1985) 261.
[38] C. Mallika, A.M. Edwin Suresh Raj, K.S. Nagaraja, O.M. Sreedharan, Thermochim. Acta 371 (2001) 95–101.
[39] J.C. Platteeuw, G. Meyer, Trans. Faraday Soc. 52 (1956) 1066.
[40] K. Atarashiya, M. Uta, M. Shimoji, K. Niwa, Bull. Chem. Soc. Jpn. 33 (1960) 706.
[41] T. Oishi, T. Hiruma, J. Moriyama, Nippon Ginzaku Gakkaishi 36 (1972) 481.
[42] G. Petot-Ervas, R. Farhi, C. Petot, J. Chem. Thermodyn. 7 (1975) 1131.
[43] T.A. Ramanarayanan, A.K. Bar, Met. Trans. B 9 (1977) 485.
[44] S. Seetharaman, L.I. Staffansson, Scand. J. Metall. 6 (1977) 143.
[45] M. Iwase, M. Yasuda, S. Miki, T. Mori, Trans. Jpn. Inst. Met. 19 (1978) 654.
[46] E. Sugimoto, S. Kuwata, Z. Kozuka, Nippon Kogyo Kaishi 98 (1982) 429.
[47] I. Karakaya, W.T. Thompson, Can. Metall. Quart. 22 (1983) 61.
[48] R. Kammel, J. Osterwald, T. Oishi, Metallwiss. Tech. 37 (1983) 141.
[49] M. Hillert, L.I. Staffansson, Acta Chem. Scand. 24 (1970) 3618–3626.